CYBERNETICS AND PHYSICS, VOL. 12, NO. 4, 2023, 282–288

DIGITAL CONTROL OF THE SYNCHRONOUS MODES OF THE TWO-ROTOR VIBRATION SET-UP

Olga P. Tomchina
Saint Petersburg State University of Architecture and Civil Engineering (SPSUACE),
2-nd Krasnoarmeiskaya St. 4, 190005, St. Petersburg, Russian Federation
otomchina@mail.ru

Article history:
Received 03.12.2023, Accepted 26.12.2023

Abstract

The work is devoted to study of the effectiveness of the algorithm for controlling the synchronization of the rotors of a vibration unit (VU) with the digital implementation of the specified algorithm. A computer study of the dynamics of a two-rotor VU with a digital implementation of the control algorithm for rotor synchronization is carried out in the MATLAB environment. As a result the permissible sampling interval for calculating discrete control values using a zero-order extrapolator circuit was estimated. Also, using modeling, a comparative analysis of the efficiency of synchronization control in digital and analog implementation of the algorithm was carried out. It is shown that with an increase in the specified operating speed of the rotors, determined by the value of the energy H^* specified in the algorithm, the permissible value of the sampling interval decreases significantly. Comparison of the VU dynamics with the same values of the parameters of the synchronization control algorithm shows that the time of synchronization and the transient process in both cases are almost the same.

1 Introduction

Currently, digital computers are an integral part of automated control systems, which makes it possible to solve a wide range of problems. For digital control of systems, it is possible to develop new methods used both at lower levels in the form of programmed algorithms, and at upper levels in the form of programs for implementing problem-oriented computational methods. When creating a control system for complex technological equipment, it is advisable to carry out computer simulation, which makes it possible to verify its performance, reliability, and investigate issues of accuracy when the equipment operates in the main operating modes.

An important class of technological equipment are vibration units used for research, testing and processing of materials in various fields of science and technology. However, automated control systems for vibration units are still rarely used due to the complexity (nonlinearity) of their dynamics and implementation [Fang et al., 2022; Huang et al., 2019; Long and Dudarenko, 2022; Tomchina, 2018; Tomchina, 2022]. The issues of digital implementation of control systems for vibration installations are even less studied; only a few works devoted to them are available in the literature [Chen and Li, 2019; Andrievsky et al., 2022; Shagniev and Fradkov, 2023].

This article is devoted to the study of the features of digital implementation and the effectiveness of the algorithm for controlling the synchronization of rotors of vibration units (VU) using computer modeling. The two-rotor mechatronic vibration stand SV-2M, developed at the Institute of Mechanical Engineering Problems of the Russian Academy of Sciences, was chosen as the object of study [Andrievskii et al., 2016]. A number of works have been devoted to the study of control issues of such a unit [Andrievskii et al., 2016; Blekhman et al., 1999], but assessment of the effectiveness of the digital implementation of rotor synchronization algorithms has not yet been considered.

2 Two-rotor vibration unit: kinematics and dynamics

Efficiency of the proposed algorithms is analyzed for 2-rotor vibration unit model with 6 degrees of freedom taking into account 3 degrees of freedom for supporting body.

The unit dynamics can be described by the Lagrange 2nd kind equations, see [Andrievskii et al., 2016; Blekhman et al., 1999] It is described below for com-

pleteness.

$$
\begin{aligned}
&m_0\ddot{x}_c - \ddot{\varphi} m_\varrho \left[\sin(\varphi+\varphi_1)+\sin(\varphi+\varphi_2)\right] - \\
&\ddot{\varphi}_1 m_\varrho \sin(\varphi+\varphi_1) - \ddot{\varphi}_2 m_\varrho \sin(\varphi+\varphi_2) - \\
&\dot{\varphi}^2 m_\varrho \left[\cos(\varphi+\varphi_1)+\cos(\varphi+\varphi_2)\right] - \\
&\dot{\varphi}_1^2 m_\varrho \cos(\varphi+\varphi_1) - \dot{\varphi}_2^2 m_\varrho \cos(\varphi+\varphi_2) - \\
&2\dot{\varphi}\dot{\varphi}_1 m_\varrho \cos(\varphi+\varphi_1) - \\
&2\dot{\varphi}\dot{\varphi}_2 m_\varrho \cos(\varphi+\varphi_2) + 2c_{01}x_c + \beta\dot{x}_c = 0; \\
&m_0\ddot{y}_c + \ddot{\varphi} m_\varrho \left[\cos(\varphi+\varphi_1)+\cos(\varphi+\varphi_2)\right] - \\
&\ddot{\varphi}_1 m_\varrho \cos(\varphi+\varphi_1) - \ddot{\varphi}_2 m_\varrho \cos(\varphi+\varphi_2) - \\
&\dot{\varphi}^2 m_\varrho \left[\sin(\varphi+\varphi_1)+\sin(\varphi+\varphi_2)\right] - \\
&\dot{\varphi}_1^2 m_\varrho \sin(\varphi+\varphi_1) - \dot{\varphi}_2^2 m_\varrho \sin(\varphi+\varphi_2) - \\
&2\dot{\varphi}\dot{\varphi}_1 m_\varrho \sin(\varphi+\varphi_1) - 2\dot{\varphi}\dot{\varphi}_2 m_\varrho \sin(\varphi+\varphi_2) + \\
&2c_{02}y_c + \beta\dot{y}_c = 0; \\
&-\ddot{x}_c m_\varrho \left[\sin(\varphi+\varphi_1)+\sin(\varphi+\varphi_2)\right] + \\
&\ddot{y}_c m_\varrho \left[\cos(\varphi+\varphi_1)+\cos(\varphi+\varphi_2)\right] + \\
&\ddot{\varphi}\left[J+J_1+J_2-2dm_\varrho\left(\cos\varphi_1-\cos\varphi_2\right)\right] + \\
&\ddot{\varphi}_1\left(J_1-dm_\varrho\cos\varphi_1\right)+\ddot{\varphi}_2\left(J_2+dm_\varrho\cos\varphi_2\right)+ \\
&\dot{\varphi}_1^2 dm_\varrho\sin\varphi_1 - \dot{\varphi}_2^2 dm_\varrho\sin\varphi_2 + 2dm_\varrho\dot{\varphi}\dot{\varphi}_1\sin\varphi_1 - \\
&2dm_\varrho\dot{\varphi}\dot{\varphi}_2\sin\varphi_2 + m_\varrho g\left[\cos(\varphi+\varphi_1)+\right. \\
&\left.\cos(\varphi+\varphi_2)\right] + c_{03}\varphi + \beta\dot{\varphi} = 0; \\
&-\ddot{x}_c m_\varrho \sin(\varphi+\varphi_1) + \ddot{y}_c m_\varrho \cos(\varphi+\varphi_1) + \\
&\ddot{\varphi}\left(J_1-dm_\varrho\cos\varphi_1\right)+\ddot{\varphi}_1 J_1 - \dot{\varphi}^2 dm_\varrho\sin\varphi_1 + \\
&m_\varrho g\cos(\varphi+\varphi_1) + k_c\dot{\varphi}_1 = M_1; \\
&-\ddot{x}_c m_\varrho \sin(\varphi+\varphi_2) + \ddot{y}_c m_\varrho \cos(\varphi+\varphi_2) + \\
&\ddot{\varphi}\left(J_2+dm_\varrho\cos\varphi_1\right)+\ddot{\varphi}_2 J_2 + \dot{\varphi}^2 dm_\varrho\sin\varphi_2 + \\
&m_\varrho g\cos(\varphi+\varphi_2) + k_c\dot{\varphi}_2 = M_2;
\end{aligned}
\tag{1}
$$

where φ_1, φ_2 are the rotation angles of the rotors measured from the horizontal position, x_c, y_c are the horizontal and vertical displacement of the supporting body from the equilibrium position, $m_i = m$, $i = 1, 2$ are the masses of the rotors, $\varrho_i = \varrho$ is the eccentricity of rotors, c_{01}, c_{02} are the horizontal and vertical spring stiffness, m_0 is the total mass of the unit, β is the damping coefficient. We will assume that rotor shafts are orthogonal to the motion of the support. J_1, J_2 are the inertia moments of the rotors, g is the gravitational acceleration, k_c is the friction coefficient in the bearings, M_1, M_2 are the motor torques (controlling variables). Kinetic and potential energies T and Π are as follows:

$$
\begin{aligned}
&T = 0.5m_0\left(\dot{x}_c^2+\dot{y}_c^2\right) + 0.5\dot{\varphi}^2\left(J+J_1+J_2-\right. \\
&\left.2dm_\varrho\left(\cos\varphi_1-\cos\varphi_2\right)\right) + 0.5J_1\dot{\varphi}_1^2 + 0.5J_2\dot{\varphi}_2^2 + \\
&\dot{\varphi}\dot{\varphi}_1\left(J_1-dm_\varrho\cos\varphi_1\right)+\dot{\varphi}\dot{\varphi}_2\left(J_2+dm_\varrho\cos\varphi_2\right) - \\
&\dot{x}_c\dot{\varphi}m_\varrho\left(\sin(\varphi+\varphi_1)+\sin(\varphi+\varphi_2)\right) + \\
&\dot{y}_c\dot{\varphi}m_\varrho\left(\cos(\varphi+\varphi_1)+\cos(\varphi+\varphi_2)\right) - \\
&\dot{x}_c\dot{\varphi}_1 m_\varrho\sin(\varphi+\varphi_1) + \dot{y}_c\dot{\varphi}_1 m_\varrho\cos(\varphi+\varphi_1) - \\
&\dot{x}_c\dot{\varphi}_2 m_\varrho\sin(\varphi+\varphi_2) + \dot{y}_c\dot{\varphi}_2 m_\varrho\cos(\varphi+\varphi_2), \\
&\Pi = m_0 g y_c + m_\varrho g\left(\sin(\varphi+\varphi_1)+\sin(\varphi+\varphi_2)\right) + \\
&c_{01}\left(x_c^2+\alpha^2\cos^2\varphi\right)^2 + c_{02}\left(y_c^2+\alpha^2\sin^2\varphi\right)^2, \\
&H = T+\Pi.
\end{aligned}
\tag{2}
$$

The parameter values correspond to the vibration stand SV-2M designed in the IPME [Andrievskii et al., 2016].

3 Integral-differential speed-gradient control algorithms for synchronization of two-rotor vibration unit

Below the necessary definitions concerning synchronization are recalled [Tomchina, 2018; Blekhman, 2000]. Frequency synchronization is defined as an exact coincidence of angular velocities of the unbalanced rotors $\omega_s = \omega_r$; $s, r = 1, \ldots, k$ [Blekhman and Fradkov, 2004]. For practice approximate synchronization conditions are more appropriate [Blekhman, 2000]

$$
|\omega_s - \omega_r| \le \varepsilon, \tag{3}
$$

where $\varepsilon > 0$ can be chosen numerically as $\varepsilon = 0.05\,\omega^*$, with a given accuracy, similar to conventional transient process measurement. However the ratio (3) may be not sufficient for synchronization, since its fulfillment does not prevent the accumulation of a phase synchronization reduced error (reduced phase shift). That is why there is a need to impose additional requirements on the system phases. To this end the notion of approximate phase synchronization is formulated as follows [Blekhman, 2000]

$$
|\varphi_s - \varphi_r - L_{sr}| < \varepsilon_1; \quad s, r = 1, \ldots, k. \tag{4}
$$

Equations (3) and (4) should hold for some $\varepsilon > 0$, $\varepsilon_1 > 0$ and some real L_{sr}.

To provide a synchronous rotation mode of unbalanced rotors for system (1), it is suggested to use speed-gradient method with an objective functional in the following form:

$$
Q(z) = \left\{0.5(1-\alpha)\left(H-H^*\right)^2 + \alpha\left(\dot{\varphi}_1 \pm \dot{\varphi}_2\right)^2\right\}, \tag{5}
$$

where $0 < \alpha < 1$ is weight coefficient; H is total mechanical energy of a system (1), H^* is the desired value of H.

The proportional-integral (PI-) speed-gradient control algorithm with the objective functional (5) is as follows [Blekhman et al., 2002; Fradkov et al., 2016]:

$$
\begin{aligned}
M_1 = &-\gamma_1\left\{(1-\alpha)\left(H-H^*\right)\dot{\varphi}_1 + \right. \\
&\left.\tfrac{\alpha}{J_1}\left(\dot{\varphi}_1 \pm \dot{\varphi}_2\right) + \tfrac{\alpha}{J_1}\left(\dot{\varphi}_1 \pm \dot{\varphi}_2 + \Delta\varphi_1\right)\right\}; \\
M_2 = &-\gamma_2\left\{(1-\alpha)\left(H-H^*\right)\dot{\varphi}_2 \pm \right. \\
&\left.\tfrac{\alpha}{2J_2}\left(\dot{\varphi}_1 \pm \dot{\varphi}_2\right) \pm \tfrac{\alpha}{2J_2}\left(\dot{\varphi}_1 \pm \dot{\varphi}_2 + \Delta\varphi_2\right)\right\},
\end{aligned}
\tag{6}
$$

where $\gamma_i > 0$, H^* is the desired value of H.

The SV-2M control system is based on a real-time computer, implemented virtually on a PC using MATLAB Simulink. The PC ensures interaction between the research operator and the stand, and the real time computer is used to collect information and control the stand in real time.

Electric motors are controlled using power frequency converters, which are connected to the real time computer via analog control lines and the RS-485 interface. To monitor the operation of electric motors, current sensors are installed in their electrical circuits. Analog signals from the sensors are sent to a special computer input

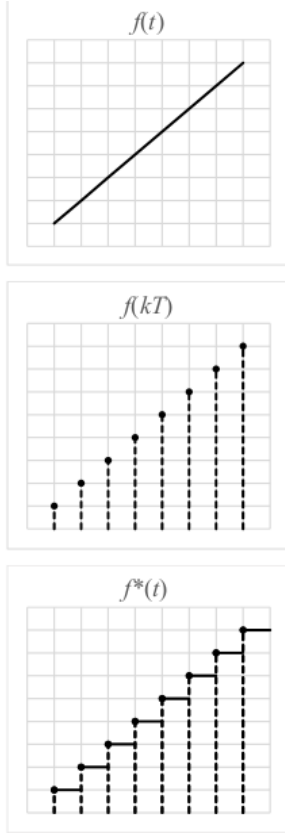

Figure 2. Type of signals when using a zero-order hold.

real time module. Pulse rotor rotation sensors are used to close the circuits of the electric motor control system. A set of sensors is used to measure the oscillatory movements of the platform and load. Linear movements of objects in the vertical plane at the points where the suspension springs are attached are measured by inductive displacement sensors. Optical displacement sensors are used to measure the movements of the platform and load in the horizontal plane. Analog signals from all displacement sensors enter the real time computer through a special analog information input module.

The control objects are also equipped with a solid-state gyroscope and accelerometer, which are used to measure the angular velocities and accelerations of objects relative to three axes. The measuring instruments have a digital output with an I^2C data transfer interface, and an auxiliary switching microcontroller is used to transfer data from the sensors to the RT computer via a standard RS-232 interface. The system architecture is focused on the use of MATLAB Simulink and Real Time Workshop tools [Andrievskii et al., 2016].

Thus, the system works with three types of signals. Firstly, with a continuous signal at the input of the control computer. Further, with a discrete signal at the computer output, which corresponds to the current calculated values of the control moments (6) and is determined at individual points in time. And, finally, a stepwise or piecewise linear continuous signal generated using an extrapolator at the input of the electric drive system. A block diagram of the conversion process using an extrapolator is shown in Fig. 1.

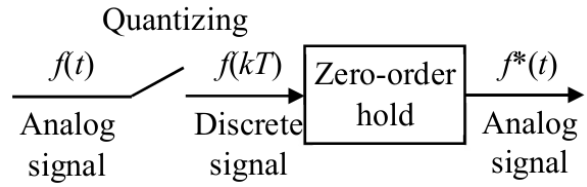

Figure 1. Block diagram of the signal conversion process.

Extrapolation is one of the ways to convert a discrete signal into a continuous signal. The simplest type of extrapolator is the zero-order extrapolator, which uses a zero-order polynomial to convert the discrete lattice input function into the step continuous function shown in Fig. 2.

Extrapolation formula

$$f^*(t) = f_k \tag{7}$$

applies in the interval $kT < t < (k+1)T$.

The analogue-code-analog conversion takes some time, which can negatively affect the stability of the entire digital control system and limit the signal frequency at the input of the electric drive system. It is advisable to first conduct a study of the performance of the algorithm (6) when controlling the SV-2M unit in various operating modes using computer simulation.

However, this raises a number of problems. One of the main problems is time quantization, which leads to a delay in updating the calculated values of control moments, since control signals in this case arrive at the object only at strictly fixed discrete moments. To build a mathematical model of vibration systems in MATLAB, there are many programs for integrating ordinary differential equations. The most effective programs for integrating complex nonlinear systems of type (1) are programs with automatic step selection ode45 and ode23. However, if the modeling of equations (1) is carried out using methods with automatic step selection, and the control torques M_1 and M_2, calculated on the computer, are formed using a zero-order extrapolator and updated at discrete equidistant time instants, that is, with a constant time step, then it is necessary to develop a special approach when modeling this digital-analog system. Namely, it is necessary to develop an algorithm that will supply control signals changing with a constant step to the input of the system (1), integrated with the automatic selection of a step that is not constant.

The block diagram of the program for simulating the dynamics of a vibration installation, described by differential equations (1) using the step-by-step integration

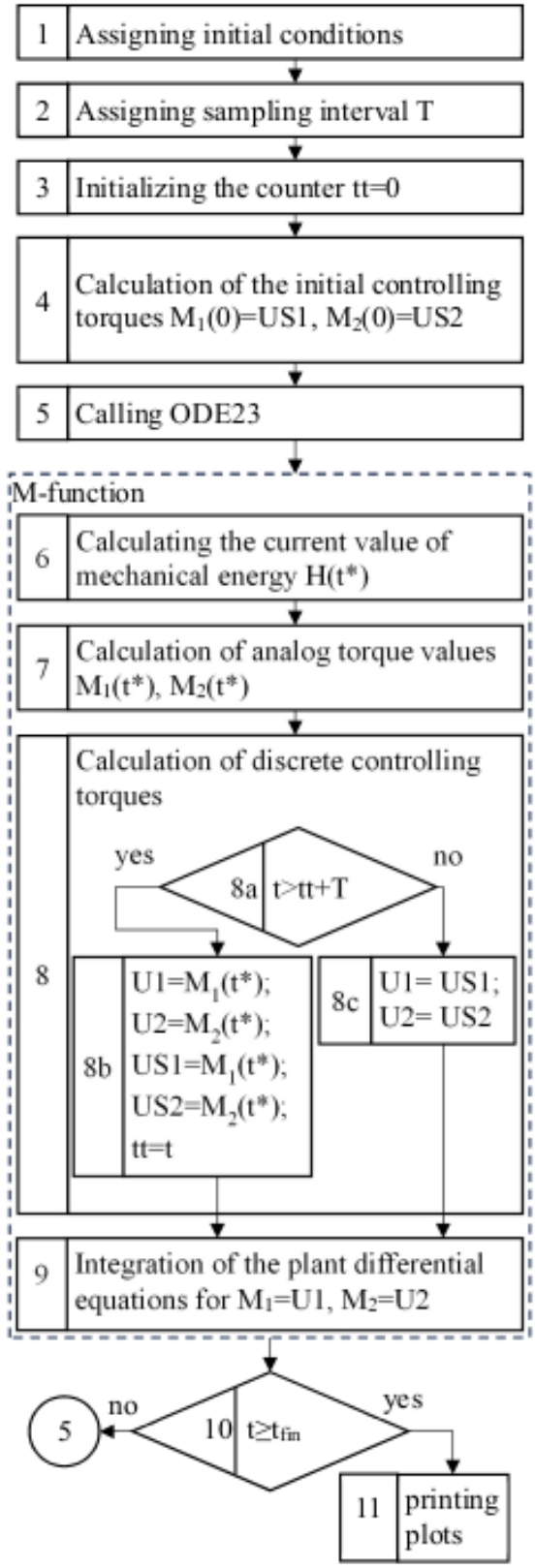

Figure 3. Scheme of the program for modeling the dynamics of the vibration unit in MATLAB.

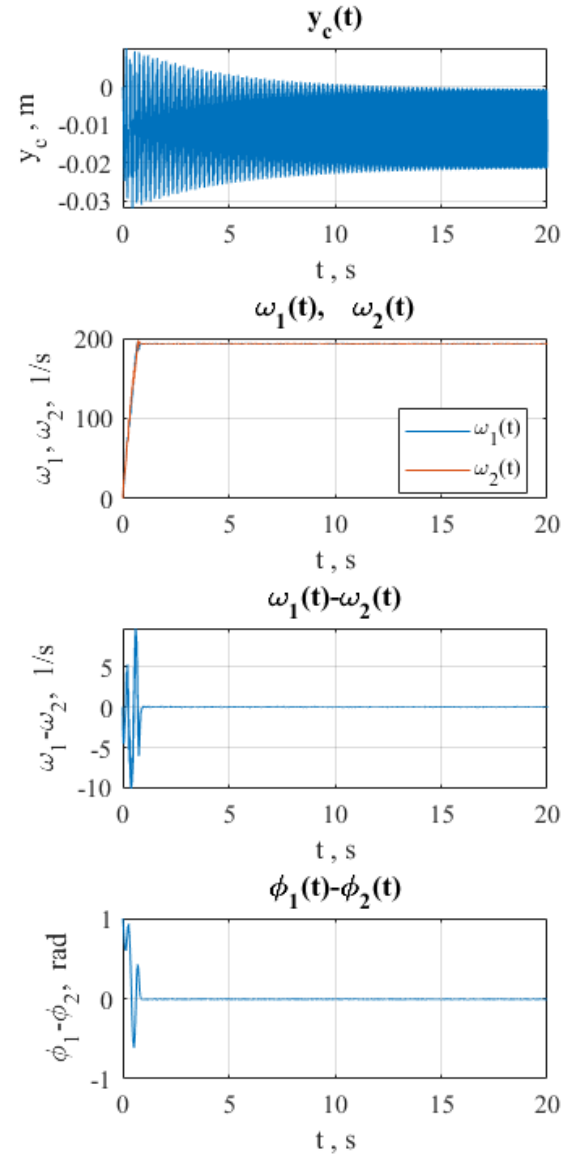

Figure 4. Simulation results with analog implementation of the control algorithm ($H^* = 500$ J, $\gamma_i = 0,012$, $\alpha_i = 0,25$).

method using the ode23 method, is presented in Figure 3.

In the M-script (blocks 1-5), global variables, numerical values of the computer parameters, parameters of the control algorithm are set, and the initial conditions and $T = \Delta t$ are the sampling step, tt is an auxiliary variable that allows you to update the value of the control signals. In the M-function (blocks 6-9) the current values of mechanical energy $H(t^*)$ and control torques are calculated using formulas that are valid when calculating analog controllers. The calculation of control moments, under the assumption that the output signal of the controller is time-quantized, is carried out in block 8, which

Table 2.

Changing parameter of the algorithm		Δt, s	t_{syn}	t_{tr}	Δt_{cr}
H^*	75	0,001	0,83	0,25	0,01
		0,01	1,18	0,26	
	150	0,001	0,88	0,32	0,01
		0,01	1,35	0,33	
	500	0,001	0,95	0,82	0,003
		0,003	1,55	1.13	
	600	0,001	1,16	0,90	0,003
		0,003	2,57	1,3	
γ_i	0,012	0,001	0,95	0,82	0,003
		0,003	1,55	1.13	
	0,025	0,001	0,93	0,81	0,003
		0,003	1,51	1.14	
	0,05	0,001	0,90	0,82	0,003
		0,003	1,48	1.14	
α_i	0,25	0,001	0,95	0,82	0,003
		0,003	1,55	1.13	
	0,025	0,001	0,95	0,83	0,003
		0,003	1,48	1.13	
	0,5	0,001	0,95	0,82	0,003
		0,003	1,51	1.13	

Table 1.

Changing parameter of the unit		t_{syn}, s	t_{tr}, s	$y_{\max}$, m
H^*, J	75	0,42	0,25	0,039
	150	0,59	0,32	0,033
	500	0,97	0,73	0,031
	600	1,17	0,78	0,032
γ_i	0,012	0,97	0,73	0,032
	0,025	0,77	0,83	0,032
	0,05	0,82	0,80	0,030
α_i	0,25	0,97	0,73	0,031
	0,025	0,76	0,63	0,031
	0,5	0,55	0,63	0,032

includes three operations. This block is constructed according to a scheme corresponding to a zero-order extrapolator. Inside the specified block, using a conditional operator, the current values of the control torques are calculated, which are assigned in accordance with the specified value of the discrete period Δt. The received signal is sent to the block for calculating the right-hand sides of differential equations. At the end, at $t \geq t_{\text{fin}}$, graphs of the main variables are printed.

4 Simulation results for study of the effectiveness of the synchronization control algorithm in digital implementation

In this section, using simulation in the MATLAB software environment, the stability of the synchronous mode of rotation of the rotors is studied and the maximum critical value of the discrete period is determined, which, first of all, should ensure acceptable processes in the system from the point of view of synchronization. The main characteristics considered in the analysis process are the time of approximate frequency-coordinate synchronization t_{syn}, at which stabilization of the rotor phase difference $\Delta\varphi(t) = \varphi_1(t) - \varphi_2(t)$ is achieved at $\varepsilon_1 = 0.05$ rad and the time of the transition process for angular velocities rotors t_{tr}. During the study, the values of the specified mechanical energy of the system H^*, which sets the values of the steady-state speeds of the rotors, were varied, as well as the algorithm parameters γ_i, α_i. $H^* = 500$ J were chosen as the basic set of parameters; $\gamma_1 = \gamma_2 = 0.012$; $\alpha_1 = \alpha_2 = 0.25$. At the first stage, a model of a vibration unit was considered for an analog implementation of a synchronization control system. Fig. 4 shows the graphs of changes in the vertical coordinate of the platform y_c, m; rotor speeds $\omega_i = \dot{\varphi}_i$, s^{-1}; as well as speed differences and rotor phase differences $\varphi_1 - \varphi_2$. In Table 1 the quantitative characteristics for the graphs of the indicated variables and the maximum amplitude of the platform vertical oscillations $y_{\max}$, m with an analog implementation of the control algorithm are presented.

The table shows that as the value of H^* increases, the synchronization time and the transition process increase; the parameters γ_i and α_i have virtually no effect on this indicator. Also, as the value of H^* and the value of γ_i increase, the maximum angle of rotation of the platform increases.

At the second stage, using modeling, the maximum critical value of the discrete period Δt_{cr} is determined, which ensures acceptable processes from the point of view of synchronization. The results of this study are presented in Table 2 and Figures 5–8.

Thus, increasing the sampling step $T = \Delta t$ leads to loss of synchronization, as can be seen in the graphs in Fig. 6 and Fig. 8. Here the steady-state phase difference exceeds the specified value ε_1, and the velocity graphs have significant beats in the steady-state mode.

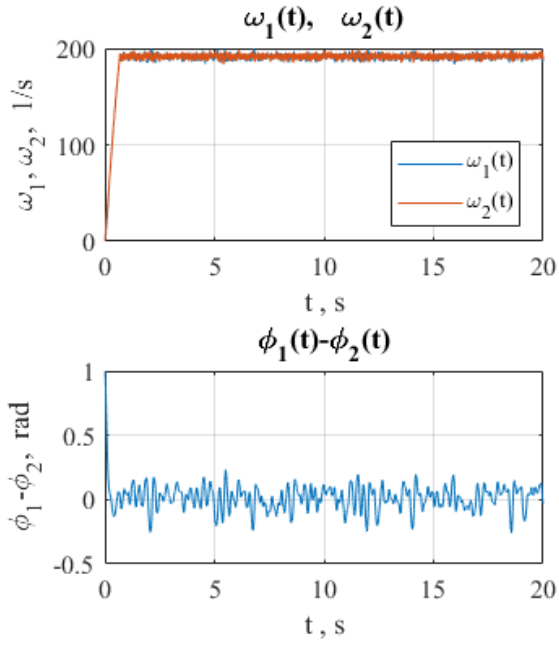

Figure 6. Simulation results for digital implementation of the control algorithm ($H^* = 500$ J, $\gamma_i = 0,012$, $\alpha_i = 0,25$, $\Delta t = 0,01$ s).

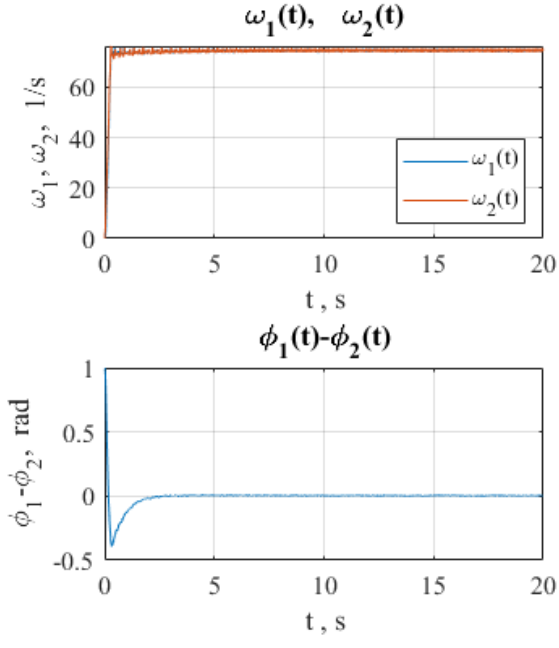

Figure 7. Simulation results for digital implementation of the control algorithm ($H^* = 75$ J, $\gamma_i = 0,012$, $\alpha_i = 0,25$, $\Delta t = 0,01$ s).

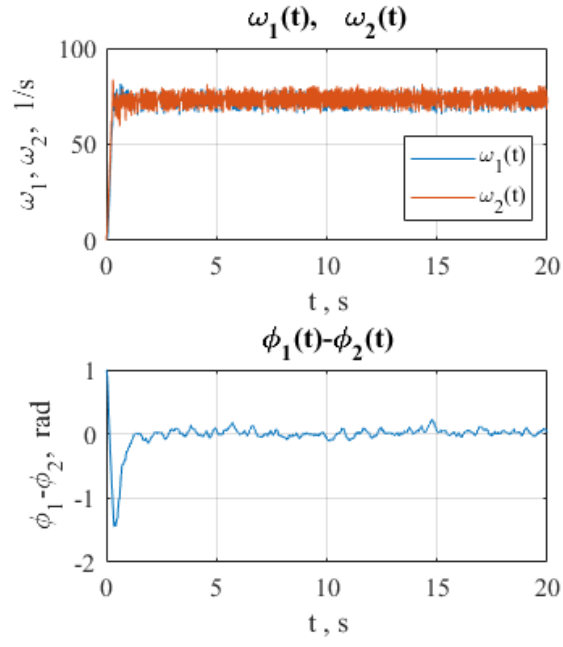

Figure 8. Simulation results for digital implementation of the control algorithm ($H^* = 75$ J, $\gamma_i = 0,012$, $\alpha_i = 0,25$, $\Delta t = 0,02$ s).

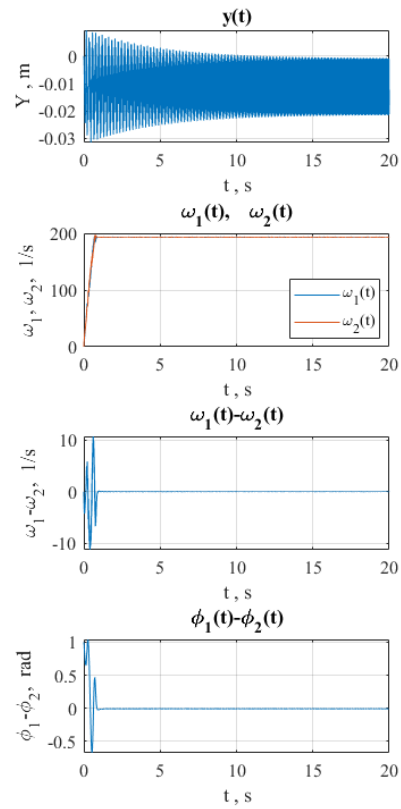

Figure 5. Simulation results for digital implementation of the control algorithm ($H^* = 500$ J, $\gamma_i = 0,012$, $\alpha_i = 0,25$, $\Delta t = 0,001$ s).

5 Conclusions

From the data presented in the table and figures it follows that with an increase in the specified operating speed of the rotors, determined by the value of the energy H^* specified in the algorithm, the permissible value of the discrete period significantly decreases. The values of synchronization time and transition process time increase with increasing specified energy H^*. Changing the parameters γ_i and α_i in the control algorithm affects the dynamics of the system to a lesser extent than varying the discrete period.

A comparison of the system dynamics with the same values of the parameters of the synchronization control algorithm shows that the time of synchronization and the transient process in both cases are almost the same. There is a slight shift in the value of the steady-state phase shift, which, however, does not lead to any differences in the average rotor speeds and the steady-state amplitude of vertical vibrations of the platform.

Future research would be devoted to study of digital control for more complex tasks: passage through resonance [Fradkov et al., 2016], taking into account material motion [Hou et al., 2022] network structure [Zaitceva et al., 2023], experimental study [Andrievsky and Boikov, 2021] etc.

References

Andrievskii, B., Blekhman, I., Blekhman, L., Boikov, V., Vasil'kov, V., and Fradkov, A. (2016). Education and research mechatronic complex for studying vibration devices and processes. *Journal of Machinery Manufacture and Reliability*, **45** (4), pp. 369–374.

Andrievsky, B. and Boikov, V. (2021). Bidirectional controlled multiple synchronization of unbalanced rotors and its experimental evaluation. *Cybernetics and Physics*, **10** (2), pp. 63—-74.

Andrievsky, B., Zaitceva, I., Boikov, V. I., and Fradkov, A. L. (2022). Digital adaptive control of unbalanced rotor velocities with anti-windup augmentation*. *IFAC-PapersOnLine*, **55** (12), pp. 258–263. 14th IFAC Workshop on Adaptive and Learning Control Systems ALCOS 2022.

Blekhman, I., Fradkov, A., Tomchina, O., and Bogdanov, D. (2002). Self-synchronization and controlled synchronization: general definition and example design. *Mathematics and Computers in Simulation (MATCOM)*, **58** (4), pp. 367–384.

Blekhman, I. I. (2000). *Vibrational Mechanics: Nonlinear Dynamic Effects, General Approach, Applications*. World Scientific.

Blekhman, I. I., Bortsov, Y. A., Burmistrov, A. A., Fradkov, A. L., Gavrilov, S. V., Kononov, O. A., Lavrov, B. P., Sokolov, P. V., Shestakov, V. M., and Tomchina, O. P. (1999). Computer-controlled vibrational setup for education and research. In *Proc. of 14th IFAC World Congress*, vol. M, pp. 193–197.

Blekhman, I. I. and Fradkov, A. L. (2004). *On general definitions of synchronization*, pp. 179–188. Singapore: World Scientific.

Chen, X. and Li, L. (2019). Phase synchronization control of two eccentric rotors in the vibration system with asymmetric structure using discrete-time sliding mode control. *Shock and Vibration*, **2019** (7481746).

Fang, P., Wang, Y., Zou, M., and Zhang, Z. (2022). Combined control strategy for synchronization control in multi-motor-pendulum vibration system. *Journal of Vibration and Control*, **28** (17-18), pp. 2254–2267.

Fradkov, A., Gorlatov, D., Tomchina, O., and Tomchin, D. (2016). Control of oscillations in vibration machines: Start up and passage through resonance. *Chaos*, **26(11)** (116310).

Hou, Y., Xiong, G., Fang, P., Du, M., and Wang, Y. (2022). Stability and synchronous characteristics of a two exciters vibration system considering material motion. *Proceedings of the Institution of Mechanical Engineers, Part K: Journal of Multi-body Dynamics*, **236** (1), pp. 15–30.

Huang, Z., Song, G., Li, Y., and Sun, M. (2019). Synchronous control of two counter-rotating eccentric rotors in nonlinear coupling vibration system. *Mechanical Systems and Signal Processing*, **114**, pp. 68–83.

Long, H. D. and Dudarenko, N. (2022). Synchronization of two-rotor vibration units using neural network-based pid controller. *Cybernetics and Physics*, **11** (3), pp. 136–144.

Shagniev, O. and Fradkov, A. (2023). Influence of discretization on the speed gradient synchronization. *Mekhatronika, Avtomatizatsiya, Upravlenie*, **24** (2), pp. 59–66.

Tomchina, O. (2018). Control of vibrational field in a cyber-physical vibration unit. *Cybernetics and Physics*, **7** (3), pp. 144–151.

Tomchina, O. (2022). Vibration field control of a two-rotor vibratory unit in the double synchronization mode. *Cybernetics and Physics*, **11** (4), pp. 246—-252.

Zaitceva, I., Andrievsky, B., and Sivachenko, L. A. (2023). Enhancing functionality of two-rotor vibration machine by automatic control. *Cybernetics and Physics*, **12** (4), pp. 289—-295.